IOP Publishing

Journal of Physics D: Applied Physics

J. Phys. D: Appl. Phys. **50** (2017) 415205 (13pp)

https://doi.org/10.1088/1361-6463/aa8794

Gas flow rate dependence of the discharge characteristics of a helium atmospheric pressure plasma jet interacting with a substrate

Wen Yan[1,2] **and Demetre J Economou**[2]

[1] School of Physics and Materials Engineering, Dalian Nationalities University, Dalian 116600, People's Republic of China

[2] Plasma Processing Laboratory, Department of Chemical and Biomolecular Engineering, University of Houston, Houston, TX 77204, United States of America

E-mail: economou@uh.edu

Received 5 July 2017, revised 12 August 2017
Accepted for publication 22 August 2017
Published 21 September 2017

Abstract

A 2D (axisymmetric) computational study of the discharge characteristics of an atmospheric pressure plasma jet as a function of gas flow rate was performed. The helium jet emerged from a dielectric tube, with an average gas flow velocity in the range 2.5–20 m s^{-1} (1 atm, 300 K) in a nitrogen ambient, and impinged on a substrate a short distance dowstream. The effect of the substrate conductivity (conductror versus insulator) was also studied. Whenever possible, simulation predictions were compared with published experimental observations. Discharge ignition and propagation in the dielectric tube were hardly affected by the He gas flow velocity. Most properties of the plasma jet, however, depended sensitively on the He gas flow velocity, which determined the concentration distributions of helium and nitrogen in the mixing layer forming in the gap between the tube exit and the substrate. At low gas flow velocity, the plasma jet evolved from a hollow (donut-shaped) feature to one where the maximum of electron density was on axis. When the gas flow velocity was high, the plasma jet maintained its hollow structure until it struck the substrate. For a conductive substrate, the radial ion fluxes to the surface were relatively uniform over a radius of ~0.4–0.8 mm, and the dominant ion flux was that of He^+. For a dielectric substrate, the radial ion fluxes to the surface peaked on the symmetry axis at low He gas flow velocity, but a hollow ion flux distribution was observed at high gas flow velocity. At the same time, the main ion flux switched from N_2^+ to He_2^+ as the He gas flow velocity increased from a low to a high value. The diameter of the plasma 'footprint' on the substrate first increased with increasing He gas flow velocity, and eventually saturated with further increases in velocity.

Keywords: atmospheric pressure plasma jet, gas flow dependence, interaction with substrate

(Some figures may appear in colour only in the online journal)

1. Introduction

Non-equilibrium (cold) atmospheric pressure plasma jets (APPJs) have attracted considerable attention owing to current and future applications in plasma medicine and materials processing [1–9]. Understanding the influence of control parameters (such as working gas flow rate, applied voltage, etc) and design features (e.g. electrode configuration, tube diameter, etc) on the plasma jet characteristics is critically important for advancing these applications [10, 11]. To this end, numerous experimental and simulation studies have contributed to a better understanding of APPJs.

In an APPJ, a discharge is formed in a capillary dielectric tube (~few mm internal diameter) by applying sinusoidal or square pulse voltages, with amplitude in the range 1–10 s of kV, at frequencies in the range of 10s of kHz to 10s of MHz. Although the discharge appears continuous to the naked eye, the luminous jet ensuing from the tube is a sequence of ionization fronts (plasma bullets), similar to streamers, that propagate with supersonic speed. As one of the important APPJ control parameters, gas flow rate affects the concentration distribution of the working gas (He in the present study) in the jet forming when the gas exits the dielectric tube into the ambient (nitrogen in this work). The mixing layer formed by inter-diffusion of the working and ambient gases has a direct influence on the space and time evolution of the ionization front, which in turn affects the APPJ characteristics, including the spatial extend of the plasma jet in free space, ion and electron density profiles, electron temperature and electric field profiles, as well as the concentration and flux distributions of ions, radicals, and other reactive species formed in the discharge.

Li *et al* [12] and Jin *et al* [13] investigated experimentally the effect of working gas flow rate on the length of an APPJ in free space (no interaction with a substrate). For low flow rates (laminar flow), the length of the luminous jet increased with flow rate. For high flow rates, however, turbulence caused the jet length to decrease with flow rate. Uchida *et al* [14] studied the gas flow rate dependence of the discharge characteristics of a He APPJ impinging on deionized water. The experimentally observed diameter of the plasma 'footprint' on the surface first increased with He gas flow rate (with concomitant increase in the total amount of charged particles transferred to the liquid) and then saturated for high gas flow rates. Hofmann *et al* [15] studied the interaction of plasma jets with different electrode configurations with conductive and dielectric substrates. The time dependent power deposition and the spatial dependence of gas temperature were investigated. The grounded substrate resulted in the most efficient power deposition and the highest gas temperature.

Experimental measurements have been complemented by modeling and simulation. The computational study of Naidis [16] showed that increasing gas flow velocity, under laminar flow conditions, led to increasing plasma bullet speed, radius, and jet propagation length in free space (no jet-substrate interaction). In the study of Sakiyama *et al*, gas flow velocity strongly affected the radial profile of atomic oxygen, formed by a plasma needle [17]. The O-atom profile changed from a solid disk at low flow rates to donut-shaped at high flow rates. On the other hand Norberg *et al* [18] studied the interaction of an APPJ with insulating or conductive substrates; their focus was not the effect of flow velocity. Breden and Raja [19] also investigated the interaction of an APPJ with an insulating substrate, paying attention on the effect of spacing between the nozzle and the substrate.

Gas flow can play an important role in carrying away the Joule heating produced in some atmospheric pressure plasmas, preventing a transition from uniform to filamentary discharge. This is not as critical in low power density APPJs for which gas heating is not significant [19–21]. Examples are APPJs designed for biomedical applications involving interaction of the jet with human tissue. Other investigators reported that gas temperature and electron density in an APPJ both decreased with increasing gas flow rate [22, 23]. The gas temperature and changes in gas temperature, however, were modest. In contrast, the effect of flow on gas cooling was important in atmospheric pressure DC microplasmas [24, 25] due to the relatively high power density (20 kW cm^{-3}) dissipated in these systems.

Despite the useful results reported in the studies discussed above and other published works, a systematic simulation study of the dynamics and structure of APPJs as a function of gas flow velocity is still lacking. Specifically, the importance of gas flow rate on the discharge characteristics during interaction of an APPJ with a conductive versus insulating substrate is an open question.

In this work, a 2D (axisymmetric) fluid model was developed to investigate the influence of gas flow velocity on a helium atmospheric pressure plasma jet, emerging in nitrogen ambient, and impinging on a conductive or insulating substrate a short distance downstream. Whenever possible, simulation predictions were compared with published experimental observations.

2. Model description

The plasma jet configuration studied in this work, shown in figure 1, was identical to that reported in a previous study [26], therefore some aspects of the system or procedures will be omitted here. The overall problem was divided into two parts: a neutral gas flow and mass transport model and a plasma dynamics model. Figure 1(a) shows the simulation domain; only half of the axisymmetric (r, z) system is shown, AG being the axis of symmetry ($r = 0$). The larger domain (ADEG) was used for the neutral gas flow and mass transport model, while the smaller domain (ACFG) was used for the plasma dynamics model. A detail of the plasma region is shown in figure 1(b). Helium gas flows through a dielectric tube (dielectric constant of 4) with 2 mm inside diameter. A high voltage (HV) ring electrode (1.5 mm axial length, 4 mm inside diameter, and 4.4 mm outside diameter) was embedded into the dielectric wall. The distance between the downstream edge of the HV electrode and the tube exit was 3.5 mm.

A trapezoidal voltage pulse with amplitude of +5 kV was applied to the ring electrode, figure 1(c). The rise and fall times of the voltage pulse were 5 ns. Following the common practice [16, 19, 20] only a single pulse was simulated. The substrate was placed 5 mm away from the tube exit, perpendicular to the jet axis. Both conductive and insulating substrates were examined. In the case of insulator (dielectric constant of 4), the thickness of the dielectric layer facing the plasma was 10 mm. This layer was assumed to lie on top of a grounded metal electrode.

The He working gas flowed through the dielectric tube and was injected into a nitrogen ambient. The Reynolds number, which characterizes the flow as laminar, transition, or turbulent, is defined by

$$\mathrm{Re} = V_{\mathrm{He}}\rho_{\mathrm{He}}d/\mu_{\mathrm{He}} \quad (1)$$

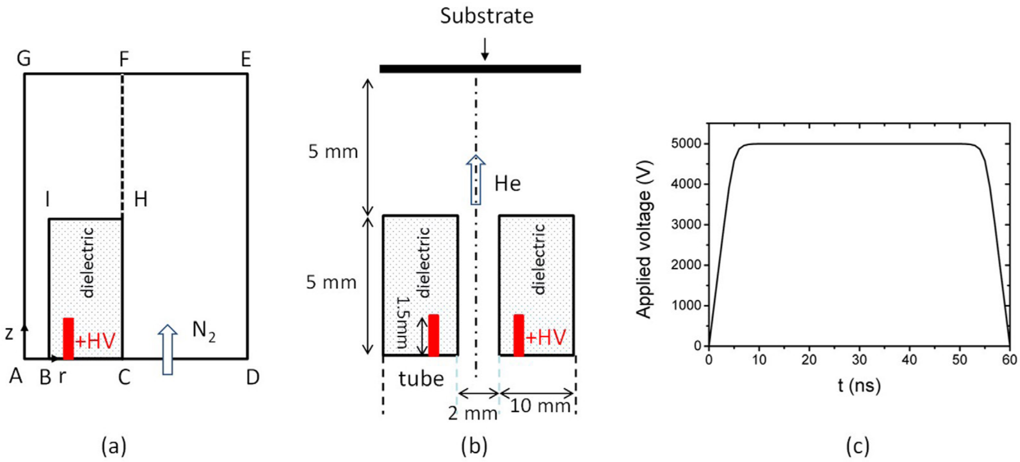

Figure 1. Schematic (not to scale) of the plasma jet configuration studied: (a) computational domain; due to axisymmetric (r, z) nature of the problem, only half of the domain is shown. The axis of symmetry is AG. Helium is fed through tubular boundary AB (1 mm radius), while N_2 enters through annular boundary CD. (b) Detail of the plasma region, not showing the region of injection of the ambient nitrogen gas. (c) Applied high voltage (HV) trapezoidal pulse.

where V_{He}, ρ_{He} and μ_{He} are characteristic flow velocity, density and viscosity of He, respectively, and d is the inside diameter of the tube. The velocity V_{He} was varied in the range 2.5 m s^{-1} to 20 m s^{-1}, corresponding to Reynolds number in the range 43–344. Under these conditions the flow is expected to be laminar [13]. To minimize the shear stress at the helium–nitrogen interface, and thus delay the onset of time dependent or turbulent flows [27], the nitrogen injection velocity ($V_{N_2} = 0.03\ V_{He}$) was increased proportionally to that of helium. The steady-state neutral gas flow and mass transport model consisted of the total mass continuity equation, the momentum conservation (Navier–Stokes) equations, and the N_2 mass balance equation. Plasma dynamics was governed by a fluid model, which was based on the species continuity equations (in the drift-diffusion approximation), the electron energy conservation equation, and Poisson's equation for the electrostatic field. The equations and boundary conditions used in this work were the same with those in a previous study [26]. As before, the gas temperature was assumed uniform at 300 K.

The mean free path for electrons (in the energy range 1–10 eV) in He, at 1 atm pressure, is $\lambda \sim 0.3\ \mu$. On the other hand, the sheath thickness (s) is a few times the Debye length λ_D where $\lambda_D = 743\sqrt{\frac{T_e}{n_e}}$ (the units of T_e and n_e are eV and cm^{-3}, respectively). For a conservative estimate ($n_e = 10^{14}$ cm^{-3} and $T_e = 5$ eV), $\lambda_D = 1.66\ \mu$. Since the mean free path is much smaller than the sheath thickness, use of the continuum (fluid) approximation is justified, even in the sheath.

The hydrodynamic flow conditions in this work correspond to a jet in laminar flow. A jet emerging in open space, however, even if it starts being laminar, will turn into a turbulent jet far enough downstream. For typical operating conditions of APPJs, the laminar-to-turbulent transition occurs ~2 cm from the nozzle (this distance depends on gas flow rate) [28]. Since the gap between the nozzle and the substrate is only 0.5 cm in the present work, we can safely assume that the jet remains laminar.

Simplified chemistry [21, 37] was used in this investigation involving reactions in the gas phase as well as recombination and quenching reactions on solid surfaces. The species considered in the model were He, metastable $He^* = He(2^3S_1)$, excimer $He_2^* = He_2(\alpha^3\sum_u)$, He^+, He_2^+, N_2, N_2^+ and electrons. The reaction mechanism is shown in table 1. The reactions used in this study were identical to those in [21, 37], except that direct ionization of ground state nitrogen, $N_2 + e \rightarrow N_2^+ + 2e$, was also included in the present work. For electron impact reactions, the corresponding rate coefficients were obtained using BOLSIG + [29], a Boltzmann equation solver. The electron transport coefficients (mobility, diffusivity) were also calculated using BOLSIG + . The cross sections used in the calculation were obtained from [30]. The transport properties for ions and metastables were obtained from [31–33]. Photo-ionization was not considered in the model; following published works [34, 35], a uniform background electron (and positive ion) density (set to 10^{13} m^{-3}) was assumed, instead. According to Breden *et al* [36], photoionization can affect the plasma bullet propagation speed but it is not needed to sustain the discharge. The secondary electron emission coefficient of solid surfaces due to bombardment by heavy species, was taken as $\gamma = 0.25$ for He^*, He_2^*, He^+ and He_2^+ and $\gamma = 0.005$ for N_2^+ [21]. The wall destruction probability of He^*, He_2^*, He^+, He_2^+, and N_2^+ was set equal to unity.

The neutral gas flow and mass transport model, as well as the plasma dynamics model were solved sequentially using COMSOL [38]. This time splitting approach is valid because of the disparate time scales of the neutral gas and plasma flows (ms versus ns). In addition, the coupling between the neutral gas flow and the plasma dynamics is often weak [19, 39, 40]. First, the neutral gas flow and mass transport model was solved to obtain the steady-state fluid velocity and the major species (He and N_2) concentration profiles. These were in turn used as input to the plasma dynamics model to obtain the time-dependent charged and neutral species concentrations as well as the electric field and electron temperature profiles. This simulation approach, also followed in [26], was similar to that reported by Naidis [16] and Breden and Raja [19, 41].

Table 1. Reactions included in this study.

Index	Reaction	Rate coefficient[a]	Energy[b]	Ref.
R1	$He + e \rightarrow He + e$	BOLSIG+		[29]
R2	$He + e \rightarrow He^* + e$	BOLSIG+	19.8	[29]
R3	$He + e \rightarrow He^+ + 2e$	BOLSIG+	24.6	[29]
R4	$He^* + e \rightarrow He^+ + 2e$	BOLSIG+	4.8	[29]
R5	$N_2 + e \rightarrow N_2^+ + 2e$	BOLSIG+	15.6	[29]
R6	$He^* + 2He \rightarrow He_2^* + He$	2.0×10^{-46} m^6 s^{-1}		[37]
R7	$He^+ + 2He \rightarrow He_2^+ + He$	1.1×10^{-43} m^6 s^{-1}		[37]
R8	$He_2^* + M \rightarrow 2He + M$	1.0×10^4 s^{-1}		[37]
R9	$2He^* \rightarrow He_2^+ + e$	1.5×10^{-15}	-17.2	[37]
R10	$2He_2^* \rightarrow He_2^+ + 2He + e$	1.5×10^{-15}	-13.8	[37]
R11	$He_2^+ + e \rightarrow He^* + He$	$8.9 \times 10^{-15}\,(T_e/T_g)^{-1.5}$	ε[c]	[37]
R12	$He^* + N_2 \rightarrow N_2^+ + He + e$	5.0×10^{-17}	-4.2	[37]
R13	$He_2^* + N_2 \rightarrow N_2^+ + 2He + e$	3.0×10^{-17}	-2.5	[37]
R14	$He_2^+ + N_2 \rightarrow N_2^+ + He_2^*$	1.4×10^{-15}		[37]
R15	$N_2^+ + e \rightarrow N_2$	$4.8 \times 10^{-13}\,(T_e/T_g)^{-0.5}$	ε[c]	[37]

Note: Species 'M' in reaction R8 represents a third-body.
[a] Rate coefficients are in m^3 s^{-1} unless noted otherwise. T_e is the electron temperature in eV, and T_g is the gas temperature in eV.
[b] Electron energy gain (negative) or loss (positive) values in eV.
[c] Local mean electron energy in eV.

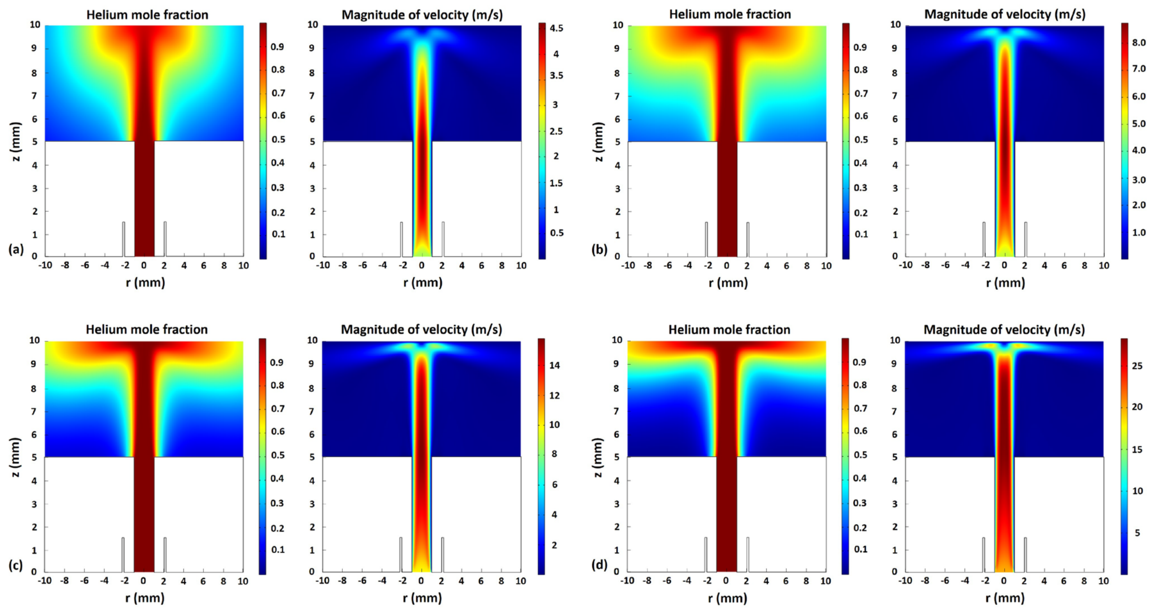

Figure 2. Profiles of helium mole fraction and magnitude of gas velocity at different He gas flow velocities: (a) 2.5 m s^{-1}, (b) 5 m s^{-1}, (c) 10 m s^{-1}, and (d) 20 m s^{-1}. Inside diameter of tube $r = 2$ mm.

3. Results and discussion

3.1. Neutral gas flow and mass transport

It has been demonstrated [16, 19, 26] that the mixing layer resulting by diffusion of the ambient gas into the helium jet emerging from the tube, is crucial to the APPJ discharge characteristics. Figure 2 shows the results of steady-state neutral gas flow and mass transport simulations for He velocities of 2.5, 5, 10, and 20 m s^{-1} (at 1 atm and 300 K). These velocities correspond to He volumetric flow rates in the range 0.47–3.77 l min^{-1}. The helium mole fraction is essentially unity inside the tube due to the large value of the Peclet number [26], preventing nitrogen counter-diffusion against the flowing helium gas. As the gas exits the tube, the helium mole fraction in the jet decreases, due to mixing (by laminar convective diffusion) of the ambient nitrogen gas into the helium jet. When the gas reaches the substrate, it flows radially outwards (stagnation point flow). The diameter of the He core of the jet shrinks as a function of axial distance from the tube exit, and then expands upon striking the substrate. As the gas flow velocity increases (from 2.5 m s^{-1} to 20 m s^{-1}), the exposure time of the helium jet to the ambient nitrogen becomes shorter, resulting in smaller penetration depth of nitrogen into the helium jet. Thus, the helium mole fraction in the axial flow

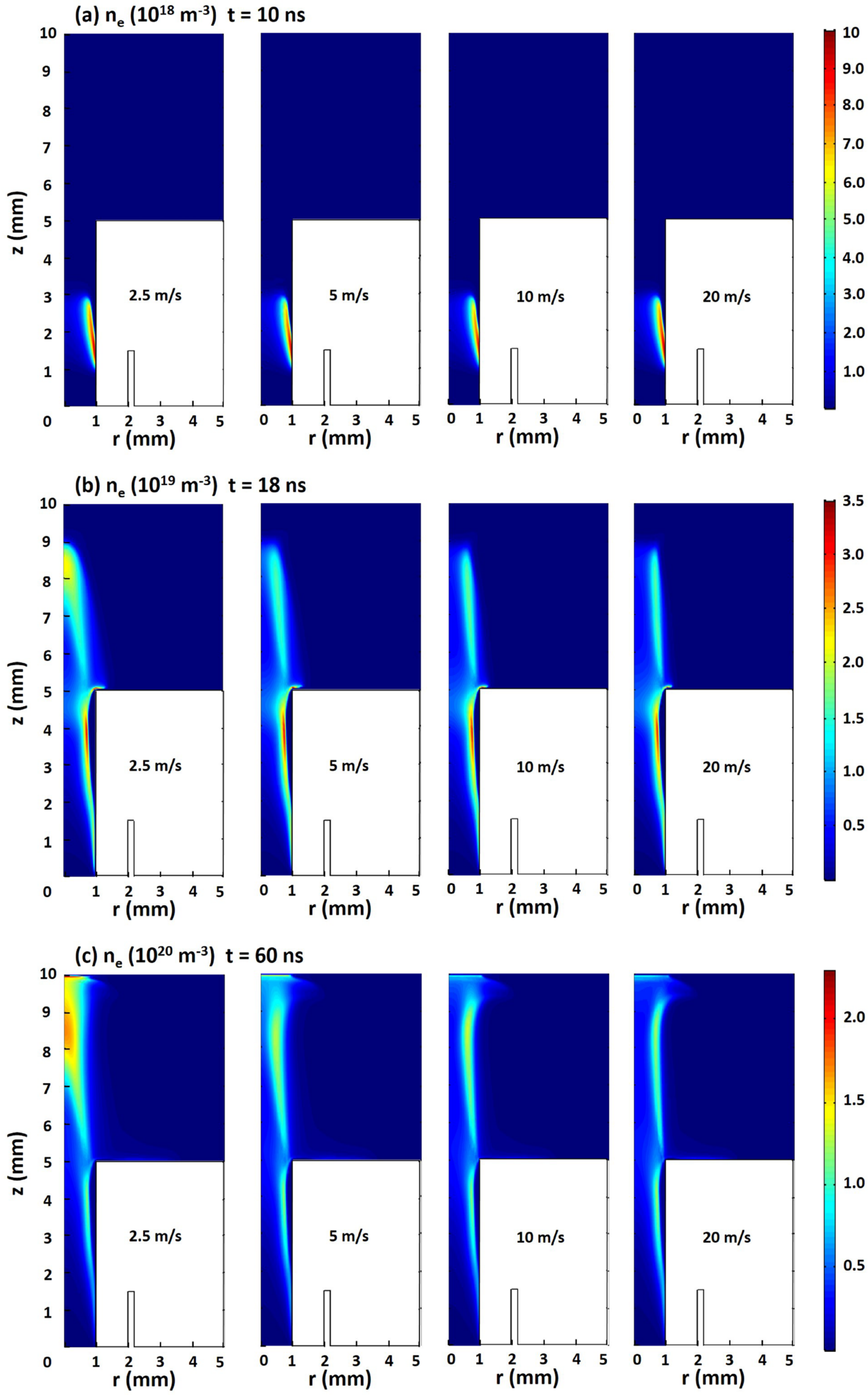

Figure 3. Spatial and temporal profiles of electron density in the plasma jet for He gas flow velocities of 2.5, 5, 10, and 20 m s^{-1}, for a conductive substrate, at different times during the HV pulse: (a) $t = 10$ ns, (b) $t = 18$ ns, (c) $t = 60$ ns. The high voltage electrode is seen protruding at $r = 2$ mm.

channel and the radial extend of the He core along the substrate surface both increase with increasing helium gas flow velocity. It should also be noted that, as expected, the mass transfer boundary layer over the substrate becomes thinner as the helium gas flow velocity increases.

3.2. Plasma dynamics for grounded conductive substrate

Figure 3 shows the spatial and temporal distributions of electron density in the plasma jet at helium gas flow velocities of 2.5, 5, 10 and 20 m s^{-1}, for a grounded conductive (e.g. metal) substrate. The peak electron density is of the order of 10^{20} m^{-3}.

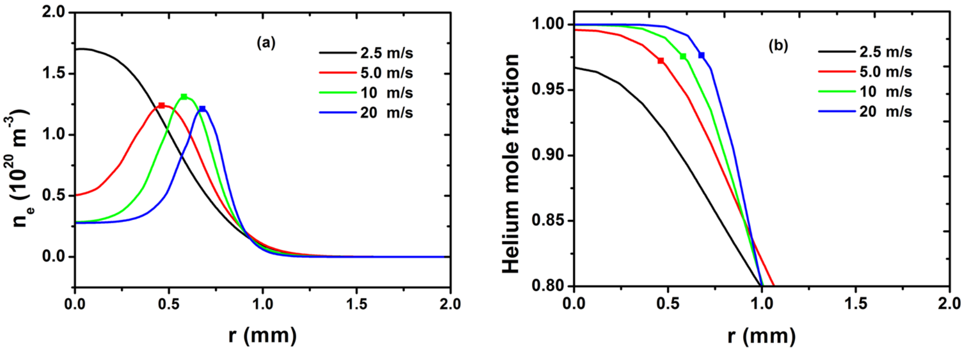

Figure 4. Radial distribution of (a) electron density, and (b) helium mole fraction in the plasma jet at axial position $z = 8.5$ mm and time $t = 60$ ns, for different He gas flow velocities. Points on the curves in (b) are at the radial positions at which the electron density is maximum, shown in panel (a). These radial positions correspond to helium mole fraction of ~0.98, a measure of the size of the helium-nitrogen mixing layer as the jet propagates in the gap between the nozzle and the substrate.

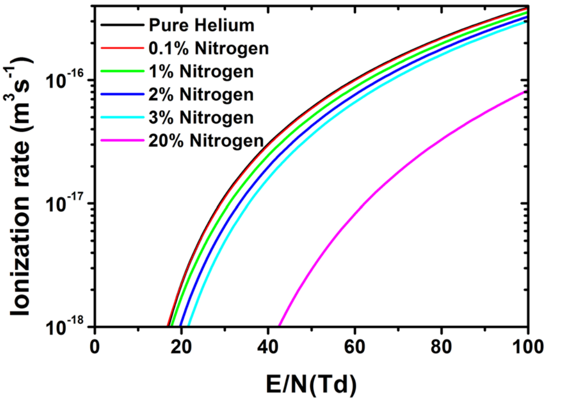

Figure 5. Direct ionization rate coefficient (k_i) as a function of the reduced electric field (E/N) in pure helium and various helium–nitrogen mixtures. Given an E/N, the k_i value of the mixture is significantly lower (compared to that of pure helium), for mixtures with mole fraction of helium less than 0.98. The lines for pure helium and 0.1% N_2 overlap with each other.

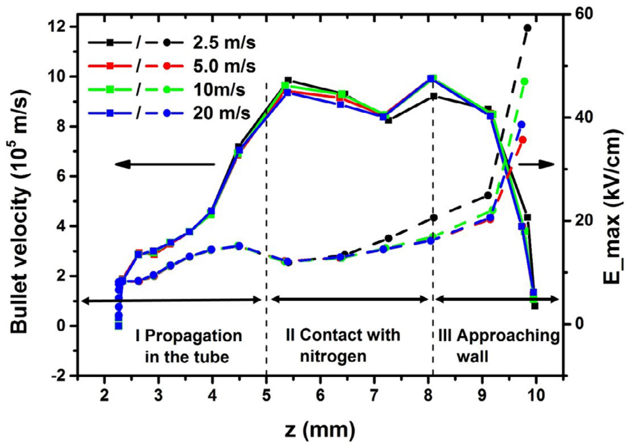

Figure 6. Plasma bullet propagation velocity (solid lines) and maximum electric field (dash lines) on axis ($r = 0$), as a function of axial position, for different He gas flow velocities. The end of the tube is at $z = 5$ mm, and the substrate (wall) is at $z = 10$ mm.

As reported in our previous work [26] and by others [42, 43], the discharge is ignited near the downstream edge of the high voltage ring electrode, where the electric field has a local maximum, and propagates inside the dielectric tube as a surface ionization wave, a short standoff distance from the tubular wall. The so-formed ionization front (also referred to as streamer or plasma bullet) exits the dielectric tube and propagates towards the cathode, guided by the helium–nitrogen mixing layer (cathode-directed streamer). Eventually, the plasma bullet strikes the substrate surface, forming a conductive channel to the substrate. Discharge initiation and propagation inside the dielectric tube is hardly affected by the helium gas flow velocity (figure 3(a)). As the discharge exits the tube (at $z = 5$ mm), variation of the gas flow velocity changes the radial structure of the plasma jet (figure 3(b)). Specifically, with an increase in He gas flow velocity, the structure of the discharge at an axial distance of 3.5 mm from the tube exit ($z = 8.5$ mm) transitions from a solid disk profile at 2.5 m s^{-1} to a donut-shaped profile at 5, 10 and 20 m s^{-1}. The transformation from a solid disk profile at low flow rate to donut-shaped profile at high flow rate is in agreement with the findings of Sakiyama *et al* [17]. The radial extend of the footprint of the plasma jet-surface interaction is only ~1 mm, even at the highest gas flow velocity examined (figure 3(c)), i.e. in the case of conductive substrate, the plasma is rather 'focused' on the substrate, in accordance with experimental observations [40].

Figure 4 shows the radial profiles of electron density (a), and helium mole fraction (b), in the plasma channel at axial position $z = 8.5$ mm, and at the end of the high voltage pulse ($t = 60$ ns) for different helium gas flow velocities. At low He gas flow velocity (2.5 m s^{-1}), the maximum electron density is on axis ($r = 0$). At high gas flow velocity, the maximum of the electron density shifts to some radial distance off axis, which increases with increasing gas flow velocity. Figure 4(b) shows that the He mole fraction is generally lower for lower gas flow velocities due to increasing exposure time of the helium jet to the nitrogen ambient and deeper penetration of nitrogen into the jet. Points on the curves in figure 4(b) are at the radial positions at which the electron density is maximum, taken from figure 4(a). As it turns out, all of these radial positions correspond to a helium mole fraction Y_{He} ~ 0.98, a measure of the extent of the helium–nitrogen mixing layer formed in the space between the tube exit and the substrate.

To explain the confinement of the plasma bullet, the direct ionization rate coefficient, k_i, (reactions R3 and R5 of table 1)

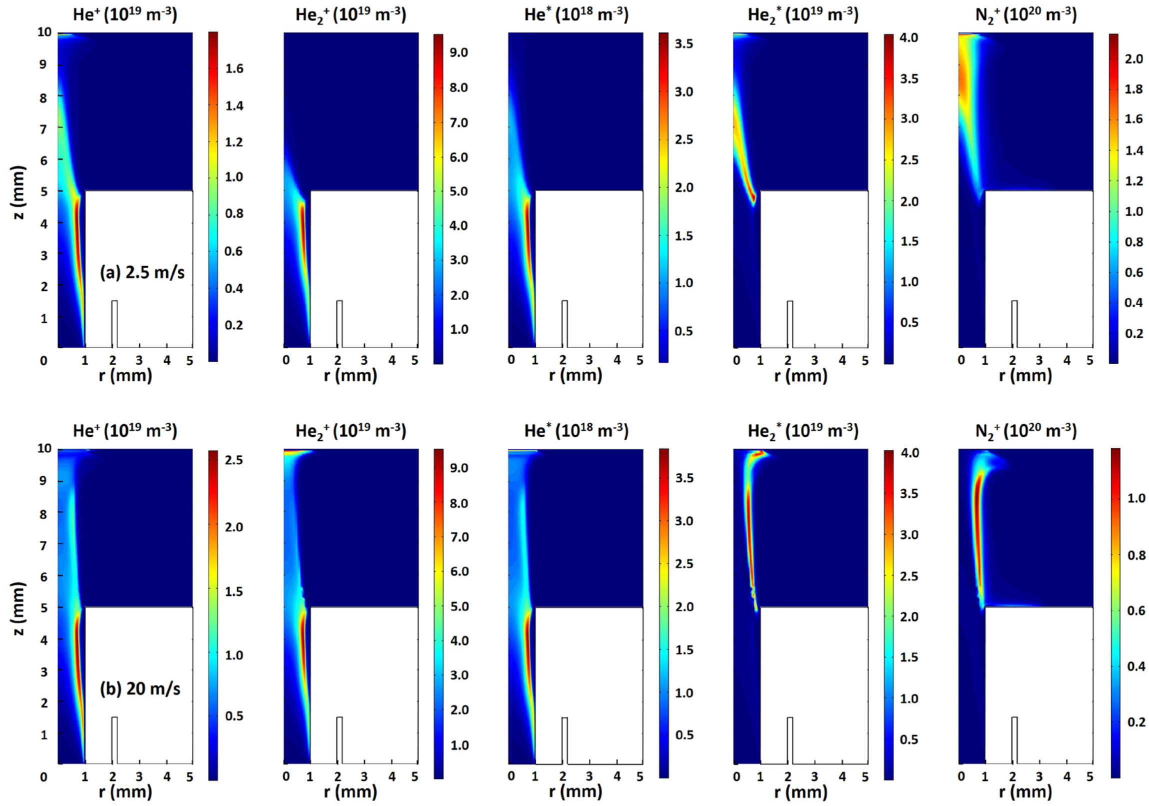

Figure 7. Spatial distribution of species density at 60 ns (end of HV pulse), for two different He gas flow velocities and conductive substrate: (top row) 2.5 m s^{-1}, (bottom row) 20 m s^{-1}.

versus reduced electric field (E/N) in pure He and He–N_2 mixtures is plotted in figure 5 [20, 44]. k_i in pure He is almost identical to that in He–N_2 mixtures with 0.1% N_2. For given E/N, k_i of the mixture is significantly lower (compared to that of pure helium), for mixtures with mole fraction of helium $Y_{He} < 0.98$. Eventually, ionization is suppressed (and the electron density drops to almost zero) when the helium mole fraction drops below ~0.8 (figure 4, at r ~ 1 mm). Thus, the radial distribution of He mole fraction in the He/N_2 mixing layer is critical for confining the plasma jet.

Figure 6 shows the propagation velocity of the plasma bullet plotted as a function of axial position along the symmetry axis ($r = 0$) for different He gas flow velocities. Three stages of propagation are identified: propagation in the dielectric tube (I), contact with the ambient gas beyond the tube exit (II), and approach to the substrate wall (III). Gas breakdown is found to occur inside the dielectric tube ~5 ns from the start of the high voltage pulse. The starting velocity of the plasma bullet (just upstream of the high voltage electrode) is low, but it steadily increases as the bullet forms and propagates inside the tube. The velocity increases to ~10^6 m s^{-1} shortly after the bullet exits the tube. This increase in the propagation velocity is thought to be, to a large part, due to Penning ionization [45]. In stage II, as the helium jet comes in contact with ambient nitrogen, the bullet velocity remains essentially unchanged. Starting at an axial location of ~8 mm, the bullet velocity decreases, as the ionization wave approaches and then strikes the substrate (located at $z = 10$ mm). Gas flow velocity has a negligible effect on the bullet velocity in the dielectric tube. A modest differentiation of the bullet velocity for different gas flow rates is observed in the free flight region between the nozzle and the wall. The insensitivity of the plasma bullet velocity on gas flow rate is in accordance with experimental measurements [46], as well as simulations by Naidis [16], which showed that within the first 5 mm of streamer propagation, after exiting the tube, the streamer velocity is essentially independent of gas flow velocity.

The maximum electric field on axis is also plotted in figure 6, as a function of position. Away from the wall, the bullet velocity generally increases with increasing electric field. Close to the wall, the electric filed increases due to the formation of a sheath [32], while the bullet (axial) velocity decreases. According to figure 2, the effect of gas flow rate on the *radial* distribution of the helium mole fraction in the jet is more dramatic than that in the *axial* distribution, due to the convective nature of the flow (high Peclet number). Variation of the radial distribution of the helium mole fraction leads to changes in the radial structure of electron density. For different He flow rates, the discharge propagates along the helium–nitrogen mixing layer, and the peak ionization rate occurs where the helium mole fraction is Y_{He} ~ 0.98. This causes a modest effect of He flow rate on the peak axial electric field, which has an important influence on the propagation velocity of the plasma bullet.

A comparison of the spatial distribution of species density at low (2.5 m s^{-1}) and high (20 m s^{-1}) He gas flow velocity, at the end of the high voltage pulse ($t = 60$ ns), is given in figure 7. He^+ is created mainly by electron impact ionization

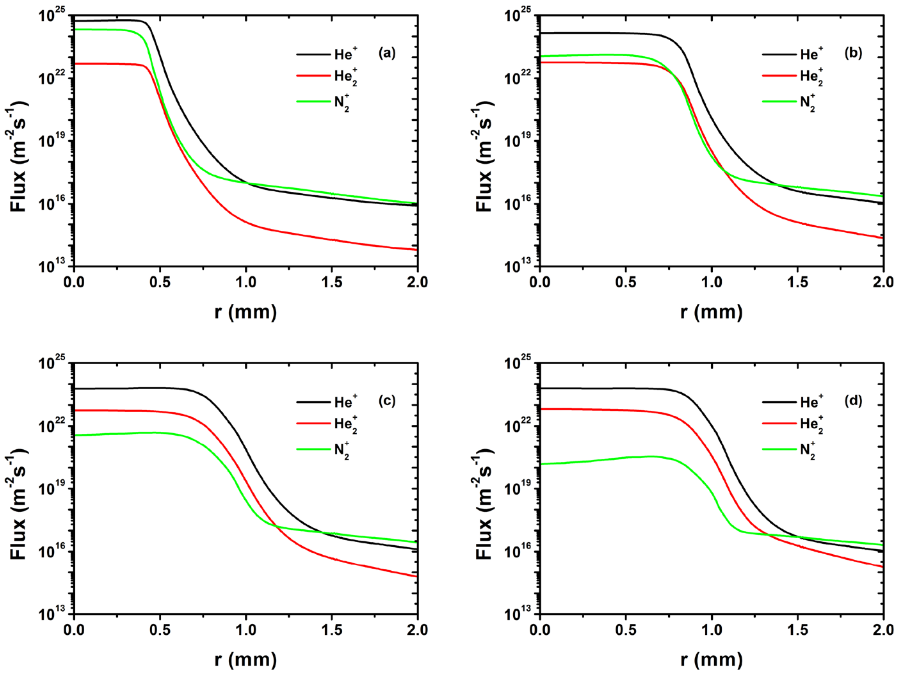

Figure 8. Radial distribution of ion fluxes ($r = 0$ is the jet axis) at the moment ($t = 21$ ns) the plasma bullet strikes the conductive substrate, for different He gas flow velocities: (a) 2.5 m s^{-1}, (b) 5 m s^{-1}, (c) 10 m s^{-1}, (d) 20 m s^{-1}.

of ground state He atoms (reaction R3, table 1). At atmospheric pressure, He^+ is rapidly converted into He_2^+ by a three-body reaction (R7). The He_2^+ density in the gap between the tube exit and the substrate ($z = 5$–10 mm), is much lower at low gas flow rates compared to high gas flow rates. This is because the lower the gas flow velocity, the higher the penetration of nitrogen into the helium jet, increasing the loss of He_2^+ through charge transfer reaction (R14). Metastable He^* is created mainly by electron impact excitation of ground state He atoms (R2). He_2^* is created mainly though charge transfer reaction (R14). Both He^* and He_2^* are quenched by Penning ionization (R12 and R13). The densities of He^* and He_2^* in the gap between the tube exit and the substrate are much lower at low gas flow velocity, compared to those at high gas flow velocity. This is because He^* and He_2^* are converted into ground state He atoms by collisions with N_2, more so at low gas flow velocity for which nitrogen penetrates deeper into the helium jet. The dominant ion in the plasma channel is N_2^+, produced in part by electron impact ionization of N_2 molecules (R15). Other paths to creating N_2^+ are Penning ionization (R12 and R13) and charge transfer (R14). The peak N_2^+ density at low He gas flow velocity is higher than that at high gas flow velocity because, again, the ambient nitrogen gas penetrates further into the helium jet at low gas flow velocity.

A significant advantage of the plasma jet is its ability to deliver high fluxes of reactive species to a surface under treatment. Figure 8 shows the radial distribution of the flux of ions onto the substrate surface, at the time when the plasma bullet touches the surface ($t = 21$ ns), for different gas flow velocities. Variation of the gas flow velocity influences the magnitude of the ion flux, but has little effect on the radial distribution of ion fluxes up to a radius of ~1 mm. When the gas flow velocity increases from 2.5 m s^{-1} to 20 m s^{-1}, the N_2^+ ion flux decreases by nearly four orders of magnitude, while the He^+ flux decreases by about one order of magnitude. For all cases, the He^+ ion flux to the surface dominates, due to the higher mobility of this species. The significant reduction of N_2^+ flux is mainly due to the lower N_2 mole fraction in the mixing layer, at the higher gas flow velocity (compare figures 2(a) and (d)). It should be noted that the fluxes shown in figure 8 are quite high because they are instantaneous fluxes at the time the plasma bullet touches the grounded substrate. Indeed, the time-average fluxes are one to two orders of magnitude lower than those shown in figure 8. Also, the extremely steep gradients of flux as a function of radius (indicating the radial extend of the bullet boundary) is noteworthy.

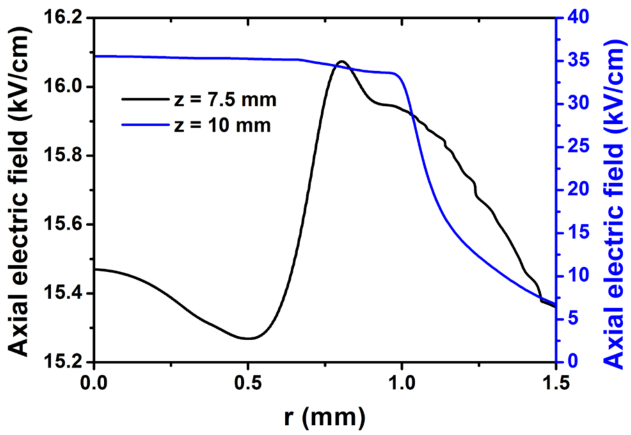

Figure 9. Time-average axial component of the electric field as a function of radius at two axial locations in the gap between the nozzle and the conducting substrate.

Figure 9 shows the time-average axial component of the electric field as a function of radius at two axial locations,

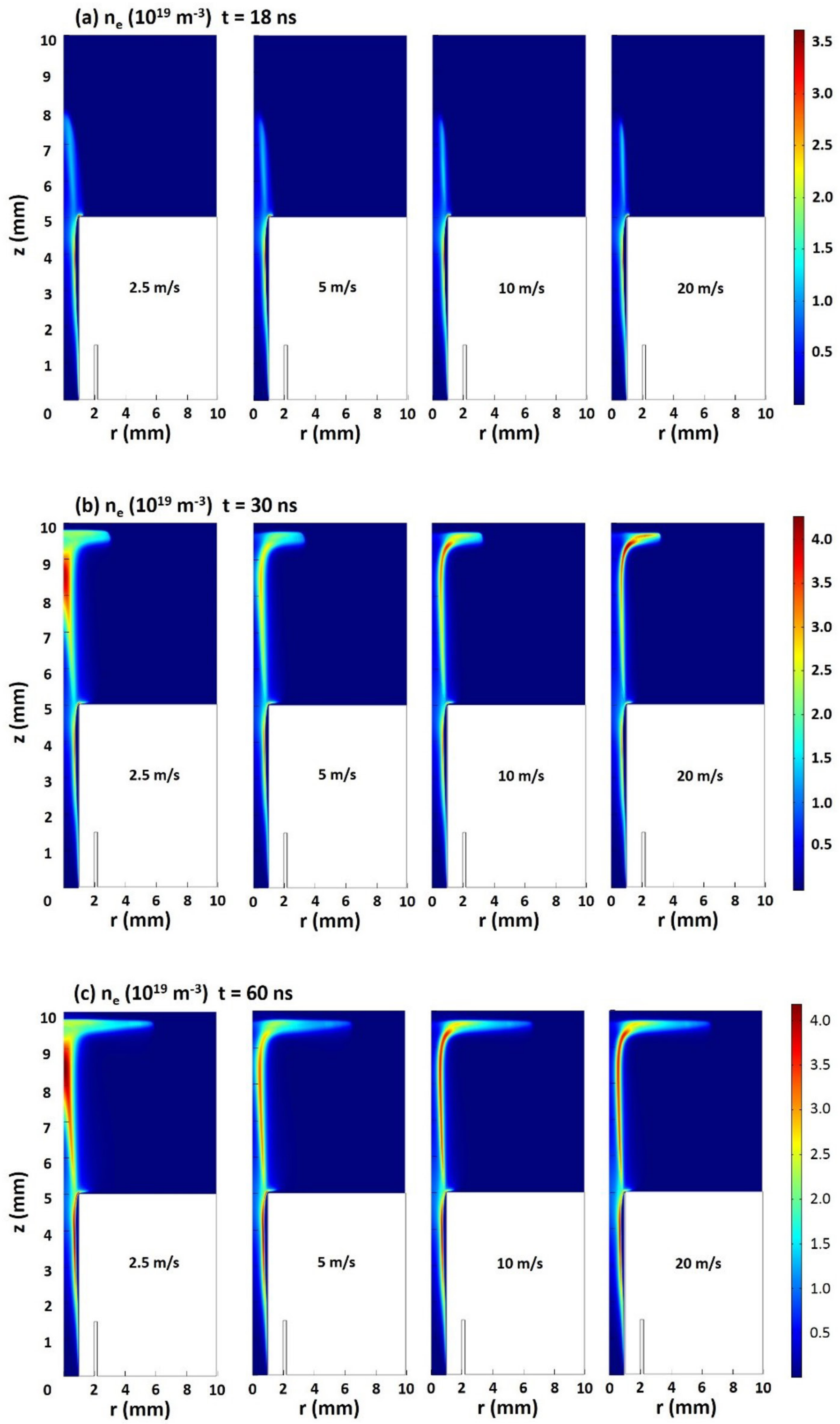

Figure 10. Spatial and temporal profiles of electron density for He gas flow velocities of 2.5, 5, 10, and 20 m s^{-1}, for an insulating substrate, at different times during the HV pulse: (a) $t = 18$ ns, (b) $t = 30$ ns, (c) $t = 60$ ns.

namely $z = 7.5$ mm (midway in the gap between the tube exit and the substrate), and $z = 10$ mm (the gas phase next to the grounded substrate). The simulated profiles are in qualitative agreement with the measurements of Sretenovic *et al* [47]. Specifically, the electric field at the substrate location has a maximum on axis, while away from the substrate the maximum electric field is found off axis.

3.3. Plasma dynamics for insulating substrate

The insulating substrate (dielectric constant of 4) was assumed to be 10 mm thick and its back-side was in contact with a grounded electrode. The effect of gas flow rate was studied keeping all other parameters constant. As discussed above, discharge initiation and propagation inside the dielectric tube was hardly affected by the helium gas flow velocity. Thus,

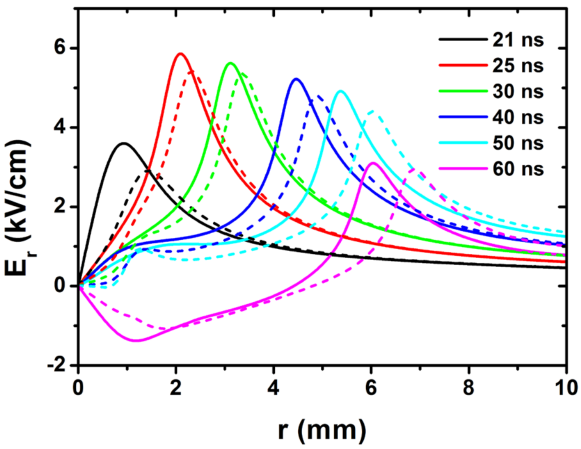

Figure 11. Magnitude of the radial component of the electric field on the dielectric substrate at different times during the HV pulse, for two He gas flow velocities. Solid lines: 2.5 m s^{-1}, dashed lines: 20 m s^{-1}.

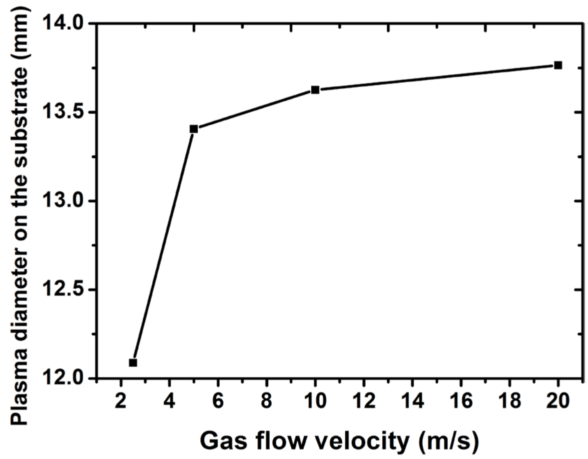

Figure 12. He gas flow velocity dependence of the diameter of the plasma footprint on the insulating substrate.

emphasis was placed on the propagation of the ionization front in the open gap between the tube exit and the substrate, and its interaction with the insulating substrate.

Figure 10 shows the spatial and temporal distribution of electron density in the plasma jet at helium gas flow velocity of 2.5, 5, 10 and 20 m s^{-1}. After exiting the dielectric tube, the ionization wave propagates along the helium–nitrogen mixing layer. At $t = 18$ ns, the ionization front crosses the middle of the gap between the tube exit and the substrate ($z = 7.5$ mm). As the plasma jet approaches the substrate, the ionization front switches direction of propagation from axial (perpendicular to the substrate) to radial (along the substrate). The radial ionization front is kept at a standoff distance above the substrate surface due to substrate charging. At low gas flow velocity, the 0.98 helium mole fraction line terminates on the z-axis (see figure 2(a)), thus the plasma jet impacts the surface at the stagnation point. As the gas flow velocity increases, the mole fraction of nitrogen in the jet is reduced. The 98% helium mole fraction line now terminates on the substrate, and the peak of the ionization front occurs at a radial distance of about 1–2 mm. When the plasma jet touches the dielectric surface, the plasma expands in the radial direction along the surface. As shown in figure 10(c), the radial propagation distance along the dielectric surface changes only moderately with He gas flow velocity.

Figure 11 shows the magnitude of the radial component of the electric field as the ionization wave propagates on the dielectric surface, for two different He gas flow velocities. At low gas flow velocity, the radial electric field reaches a maximum at radius $r = 2$ mm, gradually decreasing beyond that radius. At the end of the applied voltage pulse ($t = 60$ ns), the radial electric field in the plasma channel behind the ionization front switches sign from positive to negative. When the applied voltage decreases to zero, the positively charged ionization front acts as an anode, and the radial electric field behind that ionization front switches direction [48]. The mean radial propagation speed of the ionization front is ~1.3×10^5 m s^{-1}, about an order of magnitude lower than the ionization front propagation speed along the axis in the space between tube exit and substrate. At high gas flow velocity, the spatio-temporal evolution of the radial electric field is similar to that at low gas flow velocity. The ionization front spreads over a moderately larger radial distance, however, and the mean radial propagation velocity slightly increases to ~1.4×10^5 m s^{-1}. Also, the magnitude of the electric filed is lower for the higher flow rate, in agreement with the findings of Wang *et al* [34].

As seen in figure 12, the radial extend of the plasma footprint on the dielectric substrate surface increases when the He gas flow velocity increases from 2.5 to 5 m s^{-1}. With further increase of the He gas flow velocity, the plasma footprint diameter increases at a slower rate and saturates at ~13.75 mm. Here, plasma footprint diameter is defined as twice the radial distance of the maximum of the radial electric field of the surface discharge at $t = 60$ ns. This behavior is in agreement with the experimental results of Uchida *et al* [14].

Figure 13 shows the radial flux distributions of positive ions on the insulating surface, at time $t = 60$ ns for different He gas flow velocities. The ion flux to the dielectric surface is a few orders of magnitude lower than that on a conductive surface. At the low gas flow velocity, (2.5 m s^{-1}) the fluxes peak on the axis of symmetry ($r = 0$), and N_2^+ ions dominate the positive ion flux. The peak flux of N_2^+ on the surface (~10^{18} m^{-2} s^{-1}), is one order of magnitude higher than the peak flux of He^+. The flux of He_2^+ is negligible due to the charge exchange reaction with nitrogen (reaction R14, table 1). By increasing the gas flow velocity to 5 m s^{-1}, the He^+ and He_2^+ fluxes increase while the N_2^+ flux decreases. The peaks of N_2^+ and He^+ fluxes shift to a radial distance off axis, and the N_2^+ flux still dominates. With further increase of the gas flow velocity, the He_2^+ flux increases rapidly due to the lower loss of He_2^+ through charge transfer reaction (R14). At high gas flow velocity, the peak flux of all positive ions is some distance from the axis of symmetry (hollow profiles). The dominant positive ion flux to the surface changes to He_2^+, and the N_2^+ flux is the lowest. Despite the fact that positive ions continue to be produced during the propagation of the radial ionization front, the ion flux delivered to the surface is relatively low. This is due to the highly inefficient delivery of charges to thick (low capacitance) dielectric surfaces [19].

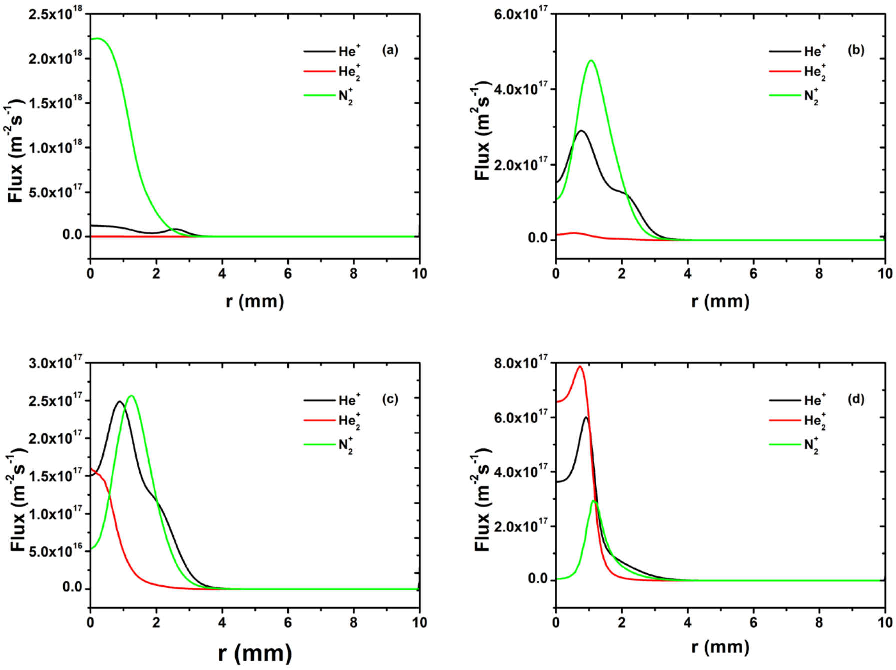

Figure 13. Radial distribution of ion fluxes onto the insulating substrate ($r = 0$ is the jet axis) at He gas flow velocities of (a) 2.5 m s^{-1}, (b) 5 m s^{-1}, (c) 10 m s^{-1}, (d) 20 m s^{-1}.

4. Summary and conclusions

A computational investigation of a non-equilibrium (cold) atmospheric pressure plasma jet (APPJ) in helium flowing inside a dielectric tube, and then emerging in nitrogen ambient was conducted, based on a 2D (axisymmetric) fluid model. Neutral gas flow and mass transport as well as plasma dynamics were included in the model. Emphasis was placed on the dependence of the discharge characteristics of the APPJ on helium gas flow velocity. The effect of the substrate conductivity (conductor versus insulator) was also studied. Results of the simulation are as follows:

(1) Discharge ignition and propagation inside the dielectric tube were hardly affected by the He gas flow velocity.
(2) The plasma bullet propagation velocity was not affected significantly by the gas flow velocity at least for short gas nozzle to substrate gap lengths (~several mm), in agreement with published results.
(3) The gas flow velocity affected mixing of the working gas in the jet with the ambient gas, influencing the plasma characteristics. Variation of the flow velocity, in the laminar flow regime, led to changes in axial and radial discharge structure, ion fluxes to the substrate and footprint diameter of the plasma-surface interaction.
(4) For a grounded conductive substrate, the ions fluxes to the surface were relatively uniform up to a few mm radius from the axis of symmetry. The dominant positive ion flux to the surface was He^+. When the He gas flow velocity was increased from 2.5 m s^{-1} to 20 m s^{-1} the diameter of the footprint of the plasma-surface interaction increased modestly, while the ion flux decreased, mainly for N_2^+ ions. The plasma footprint was lower (i.e. the plasma was more 'focused') on the conductive versus the insulating substrate, in agreement with experiments.
(5) For an insulating substrate, backed by a grounded metal conductor, and for low gas flow velocity (0.5 m s^{-1}), the ion fluxes to the surface peaked on axis, and the dominant ion flux to the substrate was that of N_2^+. When the gas flow velocity increased to 20 m s^{-1}, the ion fluxes peaked off-axis, and the dominant ion flux to the surface changed to He_2^+. The diameter of the footprint of the plasma-surface interaction first increased and then reached a plateau with increasing gas flow velocity, again in agreement with experiments.

In this work, only a single high voltage pulse was simulated starting from no plasma as initial condition. In practice, a train of pulses is applied with a predetermined time between successive pulses (interpulse period, τ_i). Thus, the simulation assumes that τ_i is very long, compared to the lifetime of species, so that the system resets to the no-plasma condition before the next pulse. Lienz and Kushner [49] studied long time chemistry in an atmospheric pressure, repetitively pulsed, dielectric barrier discharge in contact with a liquid film over tissue. They showed that the electron temperature and the positive ion densities were not affected by the number of pulses applied. In contrast, the densities of some neutrals and negative ions depended on the number of pulses. Species with lifetime much shorter than τ_i will decay before the next pulse. Species with lifetime comparable to τ_i will reach a periodic steady state after several pulses. Stable species having a lifetime much longer than τ_i will accumulate with successive pulses, eventually reaching a steady state after a large number of pulses.

Acknowledgments

This work was supported by the Department of Energy, Office of Fusion Energy Science, contract DE-SC0001319. Wen Yan is grateful to the National Natural Science Foundation of China under grant No. 11705022 for a study abroad grant.

References

[1] Mitić S, Philipps J and Hofmann D 2016 Atmospheric pressure plasma jet for liquid spray treatment *J. Phys. D: Appl. Phys.* **49** 205202
[2] Norberg S A, Johnsen E and Kushner M J 2016 Helium atmospheric pressure plasma jets interacting with wet cells: delivery of electric fields *J. Phys. D: Appl. Phys.* **49** 185201
[3] Lee J H, Choi E H, Kim K M and Kim K N 2016 Effect of non-thermal air atmospheric pressure plasma jet treatment on gingival wound healing *J. Phys. D: Appl. Phys.* **49** 075402
[4] Engelhardt M, Pothiraja R, Kartaschew K, Bibinov N, Havenith M and Awakowicz P 2016 Interaction of an argon plasma jet with a silicon wafer *J. Phys. D: Appl. Phys.* **49** 145201
[5] Liu D X, Bruggeman P, Iza F, Rong M Z and Kong M G 2010 Global model of low-temperature atmospheric-pressure He + H_2O plasmas *Plasma Sources Sci. Technol.* **19** 025018
[6] Keidar M and Robert E 2016 Preface to special topic: plasmas for medical applications *Phys. Plasmas* **22** 121901
[7] Li Y, Kang M H, Uhm H S, Lee G J, Choi E H and Han I 2017 Effects of atmospheric-pressure plasma and plasma activated nitric oxide water on cervical cancer cells *Sci. Rep.* **7** 45781
[8] Graves D B 2017 Low temperature plasma biomedicine: a tutorial review *Phys. Plasmas* **21** 080901
[9] Lu X, Naidis G V, Laroussi M, Reuter S, Graves D B and Ostrikov K 2016 Reactive species in non-equilibrium atmospheric-pressure plasmas: generation, transport, and biological effects *Phys. Rep.* **630** 1–84
[10] Lu X, Naidis G V, Laroussi M and Ostrikov K 2014 Guided ionization waves: theory and experiments *Phys. Rep.* **540** 123–66
[11] Laroussi M and Akan T 2007 Arc-free atmospheric pressure cold plasma jets: a review *Plasma Process. Polym.* **4** 777–88
[12] Li Q, Li J T, Zhu W C, Zhu X M and Pu Y K 2009 Effects of gas flow rate on the length of atmospheric pressure nonequilibrium plasma jets *Appl. Phys. Lett.* **95** 141502
[13] Jin D J, Uhm H S and Cho G 2013 Influence of the gas-flow Reynolds number on a plasma column in a glass tube *Phys. Plasmas* **20** 083513
[14] Uchida G, Nakajima A, Takenaka K, Koga K, Shiratani M and Setsuhara Y 2015 Gas flow rate dependence of the discharge characteristics of a plasma jet impinging onto the liquid surface *IEEE Trans. Plasma Sci.* **43** 4081–7
[15] Hofmann S, Van Gils K, Van Der Linden S, Iseni S and Bruggeman P 2014 Time and spatial resolved optical and electrical characteristics of continuous and time modulated RF plasmas in contact with conductive and dielectric substrates *Eur. Phys. J.* D **68** 56
[16] Naidis G V 2012 Modeling of helium plasma jets emerged into ambient air: Influence of applied voltage, jet radius, and helium flow velocity on plasma jet characteristics *J. Appl. Phys.* **112** 103304
[17] Sakiyama Y, Knake N, Schröder D, Winter J, Schulz-von der Gathen V and Graves D B 2010 Gas flow dependence of ground state atomic oxygen in plasma needle discharge at atmospheric pressure *Appl. Phys. Lett.* **97** 151501
[18] Norberg S A, Johnsen E and Kushner M J 2015 Helium atmospheric pressure plasma jets touching dielectric and metal surfaces *J. Appl. Phys.* **118** 013301
[19] Breden D and Raja L L 2014 Computational study of the interaction of cold atmospheric helium plasma jets with surfaces *Plasma Sources Sci. Technol.* **23** 065020
[20] Boeuf J-P, Yang L L and Pitchford L C 2013 Dynamics of a guided streamer ('plasma bullet') in a helium jet in air at atmospheric pressure *J. Phys. D: Appl. Phys.* **46** 015201
[21] Sakiyama Y and Graves D B 2009 Neutral gas flow and ring-shaped emission profile in non-thermal RF-excited plasma needle discharge at atmospheric pressure *Plasma Sources Sci. Technol.* **18** 025022
[22] Li S-Z, Huang W-T and Wang D 2009 The effect of gas flow on argon plasma discharge generated with a single-electrode configuration at atmospheric pressure *Phys. Plasmas* **16** 093501
[23] Qian M, Ren C, Wang D, Zhang J and Wei G 2010 Stark broadening measurement of the electron density in an atmospheric pressure argon plasma jet with double-power electrodes *J. Appl. Phys.* **107** 063303
[24] Wang Q, Doll F, Donnelly V M, Economou D J, Sadeghi N and Franz G F 2007 Experimental and theoretical study of the effect of gas flow on gas temperature in an atmospheric pressure microplasma *J. Phys. D: Appl. Phys.* **40** 4202–11
[25] Wang Q, Economou D J and Donnelly V M 2006 Simulation of a direct current microplasma discharge in helium at atmospheric pressure *J. Phys. D: Appl. Phys.* **100** 023301
[26] Yan W and Economou D J 2016 Simulation of a non-equilibrium helium plasma bullet emerging into oxygen at high pressure (250–760 Torr) and interacting with a substrate *J. Appl. Phys.* **120** 123304
[27] Satti R P and Agrawal A K 2006 Flow structure in the near-field of buoyant low-density gas jets *Int. J. Heat Fluid Flow* **27** 336–47
[28] Xian Y Bin, Qaisrani M H, Yue Y F and Lu X P 2016 Discharge effects on gas flow dynamics in a plasma jet *Phys. Plasmas* **23** 103509
[29] Hagelaar G and Pitchford L 2005 Solving the Boltzmann equation to obtain electron transport coefficients and rate coefficients for fluid models *Plasma Sources Sci. Technol.* **14** 722–33
[30] SIGLO Database www.lxcat.net (Accessed: 7 June 2015)
[31] Yan W, Liu F, Sang C and Wang D 2014 Two-dimensional numerical study of two counter-propagating helium plasma jets in air at atmospheric pressure *Phys. Plasmas* **21** 063505
[32] Yan W, Liu F, Sang C and Wang D 2014 Two-dimensional modeling of the cathode sheath formation during the streamer-cathode interaction *Phys. Plasmas* **21** 013504
[33] Bourdon A, Darny T, Pechereau F, Pouvesle J-M, Viegas P, Iséni S and Robert E 2016 Numerical and experimental study of the dynamics of a μs helium plasma gun discharge with various amounts of N_2 admixture *Plasma Sources Sci. Technol.* **25** 035002
[34] Wang L, Zheng Y and Jia S 2016 Numerical study of the interaction of a helium atmospheric pressure plasma jet with a dielectric material *Phys. Plasmas* **23** 103504
[35] Hasan M I and Bradley J W 2015 Computational study of the afterglow in single and sequential pulsing of an atmospheric-pressure plasma jet *Plasma Sources Sci. Technol.* **24** 055015
[36] Breden D, Miki K and Raja L L 2011 Computational study of cold atmospheric nanosecond pulsed helium plasma jet in air *Appl. Phys. Lett.* **99** 111501
[37] Sakiyama Y and Graves D B 2007 Nonthermal atmospheric rf plasma in one-dimensional spherical coordinates: asymmetric sheath structure and the discharge mechanism *J. Appl. Phys.* **101** 073306
[38] COMSOL 5.0 2014 (Burlington, MA: COMSOL)

[39] Lu X, Jiang Z, Xiong Q, Tang Z and Pan Y 2008 A single electrode room-temperature plasma jet device for biomedical applications *Appl. Phys. Lett.* **92** 151504
[40] Walsh J L, Shi J J and Kong M G 2006 Contrasting characteristics of pulsed and sinusoidal cold atmospheric plasma jets *Appl. Phys. Lett.* **88** 171501
[41] Breden D, Miki K and Raja L L 2012 Self-consistent two-dimensional modeling of cold atmospheric-pressure plasma jets/bullets *Plasma Sources Sci. Technol.* **21** 034011
[42] Jánský J and Bourdon A 2011 Simulation of helium discharge ignition and dynamics in thin tubes at atmospheric pressure *Appl. Phys. Lett.* **99** 161504
[43] Liu X Y, Pei X K, Lu X P and Liu D W 2014 Numerical and experimental study on a pulsed-dc plasma jet *Plasma Sources Sci. Technol.* **23** 035007
[44] Naidis G V 2011 Modelling of plasma bullet propagation along a helium jet in ambient air *J. Phys. D: Appl. Phys.* **44** 215203
[45] Wu S, Lu X and Pan Y 2014 On the mechanism of acceleration behavior of plasma bullet *Phys. Plasmas* **21** 073509
[46] Uchida G, Takenaka K, Kawabata K and Setsuhara Y 2015 Influence of He gas flow rate on optical emission characteristics in atmospheric dielectric-barrier-discharge plasma jet *IEEE Trans. Plasma Sci.* **43** 737–44
[47] Sretenovic G B and Krstic I B 2017 Spectroscopic measurement of electric field in atmospheric-pressure plasma jet operating in bullet mode *Appl. Phys. Lett.* **99** 161502
[48] Karakas E, Akman M A and Laroussi M 2012 The evolution of atmospheric-pressure low-temperature plasma jets: jet current measurements *Plasma Sources Sci. Technol.* **21** 034016
[49] Lietz A M and Kushner M J 2016 Air plasma treatment of liquid covered tissue: long timescale chemistry *J. Phys. D: Appl. Phys.* **49** 425204